Fluorescent Probes

International Edition: DOI: 10.1002/anie.201507031
German Edition: DOI: 10.1002/ange.201507031

Highly Efficient Far Red/Near-Infrared Solid Fluorophores: Aggregation-Induced Emission, Intramolecular Charge Transfer, Twisted Molecular Conformation, and Bioimaging Applications

Hongguang Lu, Yadan Zheng, Xiaowei Zhao, Lijuan Wang, Suqian Ma, Xiongqi Han, Bin Xu, Wenjing Tian, and Hui Gao**

Abstract: *The development of organic fluorophores with efficient solid-state emissions or aggregated-state emissions in the red to near-infrared region is still challenging. Reported herein are fluorophores having aggregation-induced emission ranging from the orange to far red/near-infrared (FR/NIR) region. The bioimaging performance of the designed fluorophore is shown to have potential as FR/NIR fluorescent probes for biological applications.*

The design and synthesis of organic fluorescent (FL) materials exhibiting highly efficient emissions in the solid state have attracted significant scientific interest.[1] Among the FL materials, far red/near-infrared (FR/NIR) fluorophores ($\lambda = 650$–900 nm)[2] play a crucial role in FL bioimaging because of its low tissue absorption and autofluorescence in the FR/NIR region, thus minimizing background interference and improving image sensitivity. However, FR/NIR fluorophores have strong intermolecular π–π interactions when either in high concentration or in the aggregation state, and the excited electrons usually decay nonradiatively, which causes either weak emissions or non-emission in aggregates.[3] The aggregation-caused quenching (ACQ) of emissions has been problematic in practice.

Recently, FL materials with aggregation-induced emission (AIE) characteristics have captivated much interest because they provide a straightforward solution to the problem of ACQ. Until now, many AIE fluorophores with highly twisted structures have been synthesized and their various applications have been explored, especially in optoelectronic and biological areas.[4] In bioimaging applications, AIE fluorophores can be immune to the limitations arising from the concentration of the dyes loaded into the nanoparticles (NPs). Actually, AIE NPs are supposed to be more emissive, as well as more resistant to photobleaching, by increasing concentration of the fluorophores loaded into the AIE NPs.[5] However, so far, the AIE fluorophores with FR/NIR emissions are still scarce, and probably arise from difficulties of molecular design and structural modifications. For the molecular design of FR/NIR AIE fluorophores, one has to consider either increasing the molecular conjugation length, or selecting a proper combination of an electron donor (D) and an acceptor (A) to yield fluorophores. In addition, the strikingly twisted structure has to be obtained to acquire AIE properties. Hence, the advancement of FR/NIR fluorophores with distinct AIE effects is still challenging. Tang et al. reported that AIE fluorophores with a red-shifted emission could be obtained by conjugation between a common AIE molecule (e.g. tetraphenylethylene) and ACQ fluorophores.[6] Ma et al. recently demonstrated a highly efficient NIR-emitting OLED based on the AIE compound PTZ-BZP, which displayed a hybridized local and charge-transfer excited state. Remarkably, the external quantum efficiency of the OLED was 1.54% and a highly radiative exciton ratio of 48% was observed.[7] Shimizu et al. demonstrated that 1,4-bis(diarylamino)-2,5-bis(4-cyanophenylethenyl) benzenes exhibited efficient NIR emissions in the solid state with a high quantum yield of 0.33.[8] However, these novel fluorophores did not have AIE properties, thus prohibiting them from being widely used for FL bioimaging and sensors.

Herein we provide a strategy for developing new AIE fluorophores (Figure 1) with efficient aggregated-state emissions ranging from the orange to FR/NIR regions. The fluorophore has a A–π–D–π–A molecular framework and the FL emission properties can be facilely tuned. By introducing the diphenylamine and cyano moieties into the molecular structure, this series of fluorophores has a highly twisted conformation owing to the steric hindrance between the two moieties, thus resulting in their distinct AIE attributes.

In particular, the fluorophores **4** and **5** exhibit high solid-state FR/NIR emissions with excellent quantum yields of 0.49 and 0.43, respectively. Moreover, in vitro and in vivo imaging of fluorophores encapsulated within Pluronic F127 was explored to showcase their potential as FR/NIR FL probes for bioimaging applications.

As shown in Figure 2A, each compound has a higher absorption peak appearing at around $\lambda = 335$ nm, which is

[*] Dr. H. Lu, Y. Zheng, Dr. X. Zhao, X. Han, Prof. H. Gao
Tianjin Key Laboratory of Organic Solar Cells and Photochemical Conversion, School of Chemistry and Chemical Engineering
Tianjin University of Technology
Tianjin 300384 (P. R. China)
E-mail: hglu@tjut.edu.cn
hgao@tjut.edu.cn
S. Ma, Dr. B. Xu, Prof. W. Tian
State Key Laboratory of Supramolecular Structure and Materials
College of Chemistry, Jilin University
Changchun 130012 (P. R. China)
Dr. L. Wang
School of materials science and engineering
Harbin Institute of Technology at Weihai
Weihai 264209 (P. R. China)
Supporting information and ORCID(s) from the author(s) for this article are available on the WWW under http://dx.doi.org/10.1002/anie.201507031.

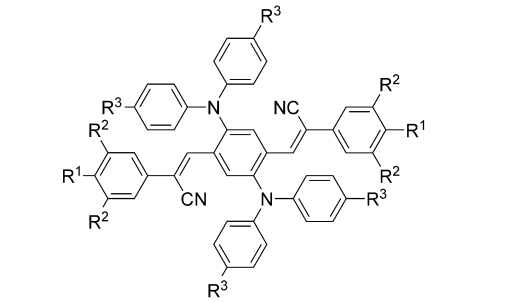

Figure 1. Structures of the fluorophores **1**–**5**.

attributed to a π–π* transition, and a weaker absorption ranging from $\lambda = 467$ to 540 nm, which is represents an intramolecular charge transfer (ICT) transition. The emission peak of the fluorophores **1**–**5** ranged from orange to the NIR region with large Stokes shifts (see Table S1 in the Supporting Information), which can be utilized to improve the signal/background ratios of fluorescence images by avoiding imaging interference between the emission and excitation.

All the fluorophores show remarkable solvent effects (see Figure S1 and Table S1). The emission peak of **4** has a bathochromic shift from $\lambda = 652$ to 677 nm with increasing solvent polarity (from cyclohexane to $CHCl_3$). These results indicate that a significant ICT transition exists in these fluorophores.[9] To better understand the ICT transitions of these fluorophores, we performed density functional theory (DFT) calculations of **4** by using the single-crystal structure determined by X-ray analysis. The molecular orbital density in the HOMO is mainly located on the central benzene rings and the diphenylamino moieties. However, the LUMO level is primarily localized on the CNC=C–C_6H_4–C=CCN framework. These results suggest a strong electron transfer within **4**.

Additionally, **1**–**5** exhibit remarkable AIE properties (see Figure S2). Typically, **4** is almost non-emissive in THF. However, when water is added, the aggregations of **4** in the THF/water mixture (>60% water) are highly emissive (Figure 2C), thus suggesting the AIE properties of **4**. The aggregations of **4** in THF/water mixtures were virtually confirmed by DLS and SEM. When the water fraction is increased to 95%, the FL intensity is about 190 times greater than that in pure THF.

The emission behaviors of **1**–**5** in the solid state were also studied. The photographs under UV light and FL spectra of **1**–**5** as crystals are given in Figure 2E. The emission peaks in powder form are red-shifted compared with those in THF/water mixtures, and the intensities are much stronger than those in aqueous mixtures. The fluorophores **1**–**5**, as crystals, exhibit fluorescence in the orange to NIR region with high Φ_F values (Figure 2E). The problematic ACQ phenomenon is more serious for red fluorophores having the elongated conjugation with large aromatic rings. Therefore, it is still a challenge to yield red emission with Φ_F values exceeding 0.3 in the solid state. It is remarkable that **4** and **5** in the solid state display strong FR/NIR emissions at $\lambda = 676$ and 686 nm, respectively, with excellent corresponding Φ_F values of 0.49 and 0.43.

Time-resolved fluorescence spectra indicate that the fluorescence lifetime (τ) of **4** as a single crystal has a single-exponential decay with a long lifetime of 17.73 ns (see Figure S3), compared to that of the $CHCl_3$ solution (5.83 ns). The single-exponential decay suggests that the

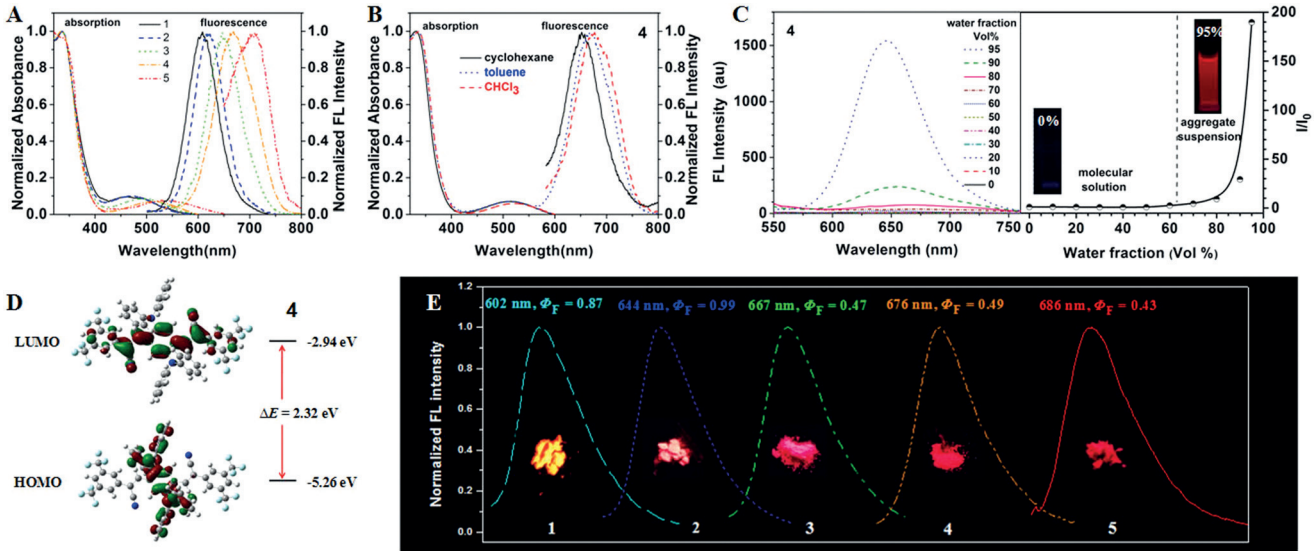

Figure 2. A) Absorption and FL spectra (solutions were excited at their absorption maxima of the longest wavelength) of **1**–**5** in toluene at 10 μM. B) Absorption and FL spectra of **4** in different solutions. C) FL spectra of **4** (50 μM) in THF/water mixtures ($\lambda_{ex} = 488$ nm) and dependence of the I/I_0 ratios on the solvent composition. D) Molecular orbital amplitude plots of HOMO and LUMO levels of **4** calculated at the B3LYP/6-31G (d, p) level of theory. E) Normalized FL spectra of **1**–**5** as crystals, and photographs of the fluorescence of **1**–**5** taken under illumination with UV light ($\lambda = 365$ nm).

excited molecules decay through a type of relaxation pathway without other competitive radiative deactivation process.[10] The radiative transition rate (K_r) and nonradiative transition rate (K_{nr}) are listed in Table S2. The K_r value of **4** (crystal) is about 24 times greater than that in a $CHCl_3$ solution, while the K_{nr} value decreases to a sixth. The increased K_r and decreased K_{nr} vaules are beneficial to increasing both τ and Φ_F by blocking a nonradiative decay pathway. Furthermore, various intermolecular interactions in the crystal could facilitate and restrict intramolecular rotation, thus leading to high K_r and Φ_F values.

The single-crystal structures indicate that all the fluorophores (**1**–**4**) show twisted molecular structures. The dihedral angles between the central benzene plane and the phenyl group, having varying substituents, of **1**, **2**, and **3** are 69.7°, 35.2°, and 68.9°, respectively. The fluorophore **4** has two crystallographically independent conformations in the crystal, and the dihedral angles between the central benzene plane and the phenyl group are 57.7° and 83.9°, respectively. Both of the conformations have a nonplanar structure. Shimizu et al. demonstrated that the 1,4-bis(diarylamino)-2,5-bis(4-cyanophenylethenyl) benzene derivatives were slightly distorted with the dihedral angles in bis(styryl)benzene framework of 21.38°.[8] Park et al. reported that the (2*Z*,2′*Z*)-3,3′-(2,5-dimethoxy-1,4-phenylene) bis(2-(4-diethylaminophenyl)acrylonitrile) formed a coplanar molecular structure in the crystal with intermolecular π–π interactions.[11] These two series of fluorophores displayed minimal AIE properties. In this work, the introduction of diphenylamine and cyano groups into the framework results in increased steric hindrance between the two moieties, and is thus beneficial for maintaining the twisted structure of this series of AIE molecules, thereby resulting in their distinct AIE attributes. No π–π stacking is observed between the adjacent molecules. In the crystals of **1**–**4**, the distances between the central benzene planes of two adjacent molecules are greater than 6.71 Å (see Figure 3 and Figure S5), which could impede intermolecular π–π interactions, and thus avoid the quenching of fluorescence in either the solid state or aggregate state.

The unique AIE property is an attractive feature for bioimaging, and could avoid the ACQ effect of organic FL probes. The Φ_F value of 4-F127 NPs dispersed in aqueous solution can reach 0.22. As shown in Figure 4, red emission is observed and randomly distributed throughout the cytoplasmic area of the A549 cells, thus showing that the 4-F127 NPs are successfully taken up by the cells. The FR/NIR emission ($\lambda > 650$ nm) of **4** was examined in vitro. Additionally, the 4-F127 NPs show a large Stokes shift of 162 nm, which can be used to avoid imaging interference between excitation and emission. The cell viability is over 85% after incubation with the 4-F127 NP suspensions at 5, 10, and 20 mg mL^{-1} for 24 hours (see Figure S7), thus suggesting that these NPs are suitable for in vitro and in vivo FR/NIR bioimaging applications.

To verify the applicability of these FR/NIR fluorophores for bioimaging in living animals, we studied the lymphatic mapping of 4-F127 NPs in ICR mice. The F-127 and 4-F127 NPs were intradermally injected into the right forepaw pads of mice. In vivo fluorescence lymphatic imaging over time is shown in Figure 5. As a control, no fluorescence signal in the area of lymph node from mice injected with F127 solutions could be observed. In contrast, in the first 5 minutes after injection with 4-F127 NPs, fluorescence signals are observed at jugular nodes, thus showing a clear lymphatic mapping and imaging. The result indicates that NPs diffused quickly from the injection site into the lymphatics. About 60 minutes later, NPs continuously migrated from the lymph node and the signal disappeared. Our results suggest that 4-F127 NPs can be used as NIR probes for potential applications in sentinel lymph node (SLN) mapping. SLN is the lymph gland that is

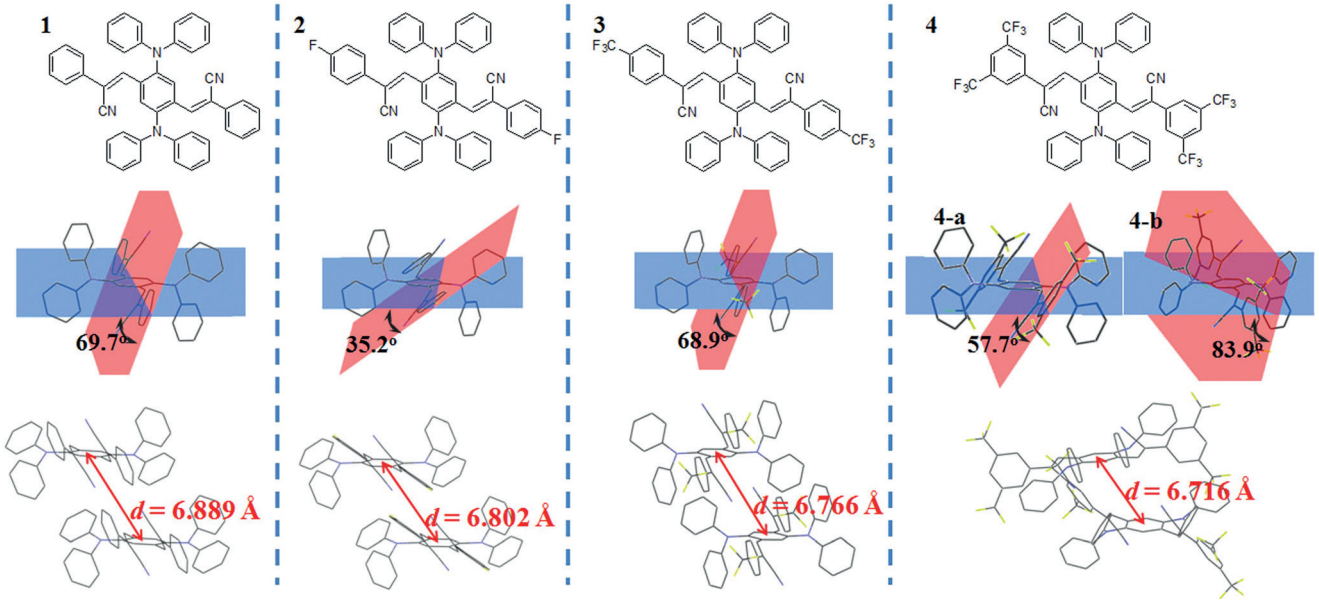

Figure 3. The dihedral angles between the central benzene plane and the phenyl group with varying substituents, and molecular stacking structures of **1**–**4** in the crystal structures. Hydrogen atoms are omitted for clarity.

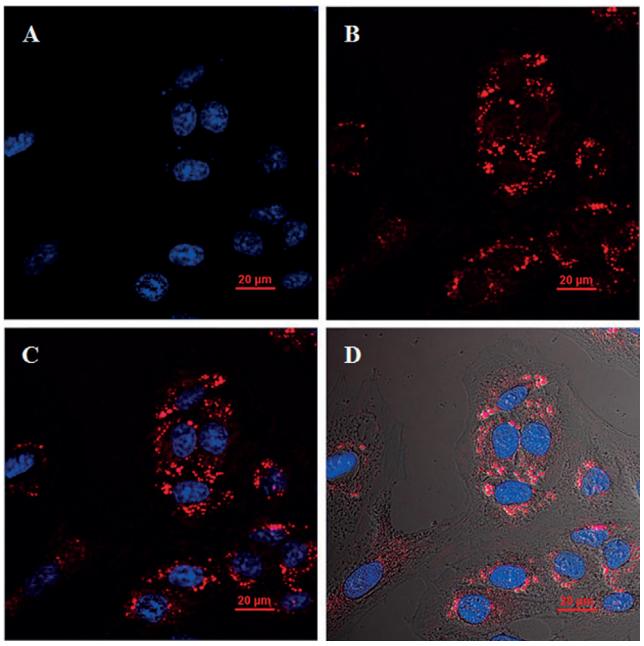

Figure 4. CLSM images of A549 cells incubated with 4-F127 NPs. A) DAPI channel. B) 4-F127 NPs channel. C) The overlay of (A) and (B). D) the overlay of (C) and bright-field images.

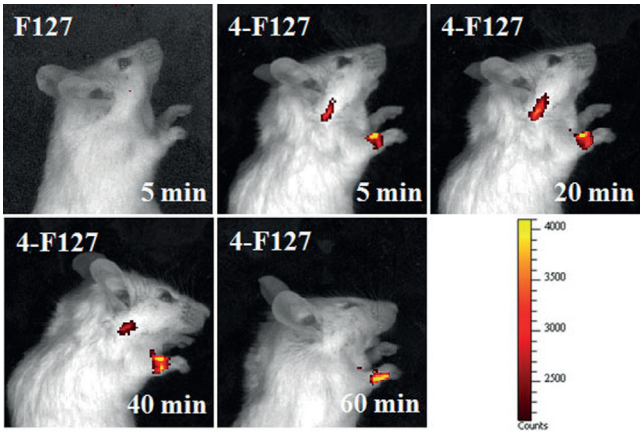

Figure 5. In vivo fluorescence images of mice with F127 and 4-F127 NPs at various time points (5, 20, 40, and 60 min).

most likely to be first invaded by cancerous cells. SLN biopsies have become a key process for cancer staging and surgery.[12] In addition, similar results are revealed for the lymphatic mapping and imaging of 5-F127 NPs (see Figure S9).

In summary, we have successfully synthesized a series of AIE fluorophores exhibiting efficient solid-state emissions in the region ranging from orange to FR/NIR. All of these fluorophores exhibit high solid-state quantum yield, and the FL color can be easily tuned by changing the substituents on the phenyl and diarylamino moieties. The fluorophores **4** and **5** exhibit high solid-state FR/NIR emissions with excellent quantum yields of 0.49 and 0.43, respectively. In vitro and in vivo imaging were explored to demonstrate the potential of the novel AIE fluorophores as FR/NIR FL probes for bioimaging applications.

Acknowledgments

We are grateful to the National Natural Science Foundation of China (21374079, 21504064), the Program for New Century Excellent Talents in University (NCET-11-1063), the Program for Prominent Young College Teachers of Tianjin Educational Committee, the Research Funds for Tianjin Educational Committee (20140501), and the Fundamental Research Funds for the Central Universities (JCKY-QKJC05) for financial support. H.L. is grateful for the support from the 131 talents program of Tianjin.

Keywords: aggregation · fluorescent probes · imaging agents · luminescence · materials science

How to cite: *Angew. Chem. Int. Ed.* **2016**, *55*, 155–159
Angew. Chem. **2016**, *128*, 163–167

[1] a) *Organic Light-Emitting Devices. Synthesis Properties and Applications* (Eds.: K. Müllen, U. Scherf), Wiley-VCH, Weinheim, **2006**; b) Q. Peng, A. Obolda, M. Zhang, F. Li, *Angew. Chem. Int. Ed.* **2015**, *54*, 7091–7095; *Angew. Chem.* **2015**, *127*, 7197–7201; c) K. Y. Pu, B. Liu, *Adv. Funct. Mater.* **2011**, *21*, 3408–3423; d) X. Zhao, Y. Li, D. Jin, Y. Xing, X. Yan, L. Chen, *Chem. Commun.* **2015**, *51*, 11721–11724; e) S. W. Thomas III, G. D. Joly, T. M. Swager, *Chem. Rev.* **2007**, *107*, 1339–1386; f) H. Bakirci, W. M. Nau, *Adv. Funct. Mater.* **2006**, *16*, 237–242.

[2] a) J. O. Escobedo, O. Rusin, S. Lim, R. M. Strongin, *Curr. Opin. Chem. Biol.* **2010**, *14*, 64–70; b) Z. Guo, S. Park, J. Yoon, I. Shin, *Chem. Soc. Rev.* **2014**, *43*, 16–29.

[3] a) J. Massin, W. Dayoub, J.-C. Mulatier, C. Aronica, Y. Bretonniere, C. Andraud, *Chem. Mater.* **2011**, *23*, 862–873; b) G. Qian, Z. Zhong, M. Luo, D. Yu, Z. Zhang, Z. Y. Wang, D. Ma, *Adv. Mater.* **2009**, *21*, 111–116; c) D. Wang, J. Qian, S. He, J. S. Park, K.-S. Lee, S. Han, Y. Mu, *Biomaterials* **2011**, *32*, 5880–5888; d) F. Ito, R. Ohta, Y. Yokota, K. Ueno, H. Misawa, T. Nagamura, *Opt. Photonics J.* **2013**, *3*, 27–31.

[4] a) Y. Hong, J. W. Y. Lam, B. Z. Tang, *Chem. Soc. Rev.* **2011**, *40*, 5361–5388; b) R. Hu, N. L. C. Leung, B. Z. Tang, *Chem. Soc. Rev.* **2014**, *43*, 4494–4562; c) Y. Dong, B. Xu, J. Zhang, X. Tan, L. Wang, J. Chen, H. Lu, S. Wen, B. Li, L. Ye, B. Zou, W. Tian, *Angew. Chem. Int. Ed.* **2012**, *51*, 10782–10785; *Angew. Chem.* **2012**, *124*, 10940–10943.

[5] a) K. Li, B. Liu, *Chem. Soc. Rev.* **2014**, *43*, 6570–6597; b) H. Lu, F. Su, Q. Mei, Y. Tian, W. Tian, R. H. Johnson, D. R. Meldrum, *J. Mater. Chem.* **2012**, *22*, 9890–9900; c) X. Zhang, X. Zhang, B. Yang, M. Liu, W. Liu, Y. Chen, Y. Wei, *Polym. Chem.* **2014**, *5*, 399–404; d) A. Shao, Y. Xie, S. Zhu, Z. Guo, S. Zhu, J. Guo, P. Shi, T. D. James, H. Tian, W. H. Zhu, *Angew. Chem. Int. Ed.* **2015**, *54*, 7275–7280; *Angew. Chem.* **2015**, *127*, 7383–7388.

[6] a) W. Qin, D. Ding, J. Liu, W. Z. Yuan, Y. Hu, B. Liu, B. Z. Tang, *Adv. Funct. Mater.* **2012**, *22*, 771–779; b) W. Qin, K. Li, G. Feng, M. Li, Z. Yang, B. Liu, B. Z. Tang, *Adv. Funct. Mater.* **2014**, *24*, 635–643; c) K. Li, W. Qin, D. Ding, N. Tomczak, J. Geng, R. Liu, J. Liu, X. Zhang, H. Liu, B. Liu, B. Z. Tang, *Sci. Rep.* **2013**, *3*, 1150–1159.

[7] a) L. Yao, S. Zhang, R. Wang, W. Li, F. Shen, B. Yang, Y. Ma, *Angew. Chem. Int. Ed.* **2014**, *53*, 2119–2123; *Angew. Chem.* **2014**, *126*, 2151–2155; b) W. Li, Y. Pan, R. Xiao, Q. Peng, S.

Zhang, D. Ma, F. Li, F. Shen, Y. Wang, B. Yang, Y. Ma, *Adv. Funct. Mater.* **2014**, *24*, 1609 – 1614.
[8] M. Shimizu, R. Kaki, Y. Takeda, T. Hiyama, N. Nagai, H. Yamagishi, H. Furutani, *Angew. Chem. Int. Ed.* **2012**, *51*, 4095 – 4099; *Angew. Chem.* **2012**, *124*, 4171 – 4175.
[9] a) E. M. Kosower, H. Dodiuk, H. Kanety, *J. Am. Chem. Soc.* **1978**, *100*, 4179 – 4188; b) G. Jones II, W. R. Jackson, C. Y. Choi, W. R. Bergmark, *J. Phys. Chem.* **1985**, *89*, 294 – 300; c) *Principles of Fluorescence Spectroscopy* (Eds.: J. R. Lakowicz), Springer, New York, **2006**, pp. 205 – 235.
[10] a) *Molecular Fluorescence Principles and Applications* (Ed.: V. Bernard), Wiley-VCH, Weinheim, **2002**; b) J. Zhang, B. Xu, J. Chen, S. Ma, Y. Dong, L. Wang, B. Li, L. Ye, W. Tian, *Adv. Mater.* **2014**, *26*, 739 – 745.
[11] M. Kim, D. R. Whang, J. Gierschner, S. Y. Park, *J. Mater. Chem. C* **2015**, *3*, 231 – 234.
[12] J. W. Jakub, S. Pendas, D. S. Reintgen, *Oncologist* **2003**, *8*, 59 – 68.

Received: July 29, 2015
Revised: October 20, 2015
Published online: November 18, 2015

